Generation of 9 MeV γ-rays by all-laser-driven Compton scattering with second-harmonic laser light

Cheng Liu,[1] Grigory Golovin,[1] Shouyuan Chen,[1] Jun Zhang,[1] Baozhen Zhao,[1] Daniel Haden,[1] Sudeep Banerjee,[1] Jack Silano,[2] Hugon Karwowski,[2] and Donald Umstadter[1,*]

[1]*Department of Physics and Astronomy, University of Nebraska-Lincoln, Lincoln, Nebraska 68588, USA*

[2]*Department of Physics and Astronomy, University of North Carolina, Chapel Hill, North Carolina 27599, USA*

**Corresponding author: donald.umstadter@unl.edu*

Received April 11, 2014; revised May 23, 2014; accepted June 6, 2014;
posted June 9, 2014 (Doc. ID 210010); published July 7, 2014

Gamma-ray photons with energy >9 MeV were produced when second-harmonic-generated laser light (3 eV) inverse-Compton-scattered from a counterpropagating relativistic (~450 MeV) laser-wakefield-accelerated electron beam. Two laser pulses from the same laser system were used: one to accelerate electrons and one to scatter. Since the two pulses play very different roles in the γ-ray generation process, and thus have different requirements, a novel laser system was developed. It separately and independently optimized the optical properties of the two pulses. This approach also mitigated the deleterious effects on beam focusing that generally accompany nonlinear optics at high peak-power levels.

OCIS codes: (340.7480) X-rays, soft x-rays, extreme ultraviolet (EUV); (320.7160) Ultrafast technology; (190.2620) Harmonic generation and mixing.
http://dx.doi.org/10.1364/OL.39.004132

High-energy γ-ray sources have applications in a wide variety of areas, including radiography of dense materials, study of nuclear processes, as well as detection of shielded nuclear materials. Currently, Bremsstrahlung-generated γ-rays are the most widely used, despite the fact that their large bandwidth results in substantial deposition of unwanted radiation dosage, and consequently, a poor signal-to-noise ratio in detection. Narrower bandwidth γ-rays are generated efficiently by means of inverse Compton scattering (ICS) [1], in which laser light is upshifted to much higher photon energy [2] by scattering from a relativistic electron beam. However, the practicality of conventional ICS sources for applications is limited by their large size, high cost, and fixed positions.

Unconventional, all-laser-driven ICS sources are currently under development. Instead of making use of electron accelerators based on conventional RF cavities, these new ICS sources are driven by laser wakefield acceleration (LWFA) [3,4]. This difference has numerous advantages. For instance, all-laser-driven ICS sources are far more compact and produce much shorter pulse durations (femtosecond). Pulses of γ-rays, electrons, and laser light are also well synchronized with each other, by virtue of being driven by the same laser system. Several all-laser-driven approaches have been demonstrated experimentally [5–7]. Our approach succeeded in producing γ-ray beams possessing MeV energy, high peak brightness, and high flux (comparable to conventional ICS) [7]. More recently, we produced quasi-monochromatic and tunable γ-ray beams using this same approach [8].

Achieving higher photon energies (>5 MeV) remains the final hurdle in order for these light sources to become comparable to conventional alternatives, and relevant to nuclear research and applications. The γ-ray energy (E) resulting from the ICS is given by $E = 4\gamma^2 E_L$, where γ is the Lorentz factor of the relativistic electron beam and E_L is the energy of the laser photons. Thus, in order to increase E, one must increase γ and/or E_L.

The former approach—increasing the electron energy—can be accomplished through use of higher laser power and longer acceleration length. However, among several other drawbacks to this approach, the γ-ray beam stability can be expected to decrease, due to the nonlinear beam propagation effects. It is also more difficult to mitigate the electron background, which degrades the signal-to-noise ratio in γ-ray detection measurements, upon which the success of most photonuclear applications depends.

The latter approach—increasing the photon energy of the scattering light—can be accomplished through use of the nonlinear optics technique of high-order harmonic generation. If the scattering laser used is doubled in optical frequency, by means of second-harmonic generation (SHG), then the energy of the γ-ray photons will also be doubled (for fixed laser fundamental frequency and electron energy). SHG is well established for lasers with long pulse duration and low peak power. However, all-laser-driven ICS involves short pulses and high peak power. Furthermore, although the two required laser pulses are amplified in the same laser system, they play very different roles in the γ-ray generation process, and thus have different requirements on their pulse characteristics.

To overcome these challenges associated with increasing E_L, we developed a novel laser system comprising separate and independent pulse compressors. This allowed the temporal characteristics of the two laser pulses to be optimized independently for the requirements of their different roles. Another advantage of this design is that it avoided the deleterious nonlinear effects encountered in previous experiments [7,8], due to placing the laser beam splitter before, rather than after the compressors, where peak power is low, rather than where it is high. These factors resulted in both optimal LWFA performance and efficient SHG conversion to focusable 400 nm light, thus yielding high γ-ray energy (>9 MeV). To the best of our knowledge, this is the first all-laser-driven ICS source to produce γ-rays with energy sufficient to be relevant to nuclear research and applications.

The experiment was conducted using the 100-TW Diocles laser system that operates on the principle of

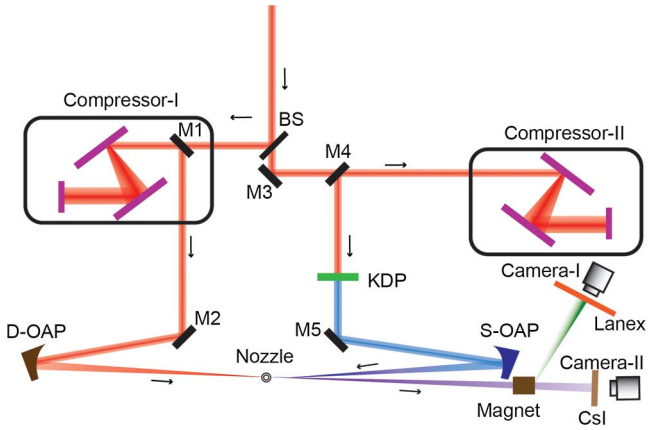

Fig. 1. Experimental setup for generation of 9 MeV γ-ray beams by all-optical ICS. BS, beam splitter; M1–M4, high-reflective 45° mirrors for 800 nm; M5, 45° dichroic mirror, high reflects 400 nm and transmits 800 nm; D-OAP, parabolic focusing mirror for the drive beam; S-OAP, parabolic focusing mirror for the scattering beam; KDP, SHG crystal; Compressor-I, compressor for the drive laser beam; Compressor-II, compressor for the scattering laser beam.

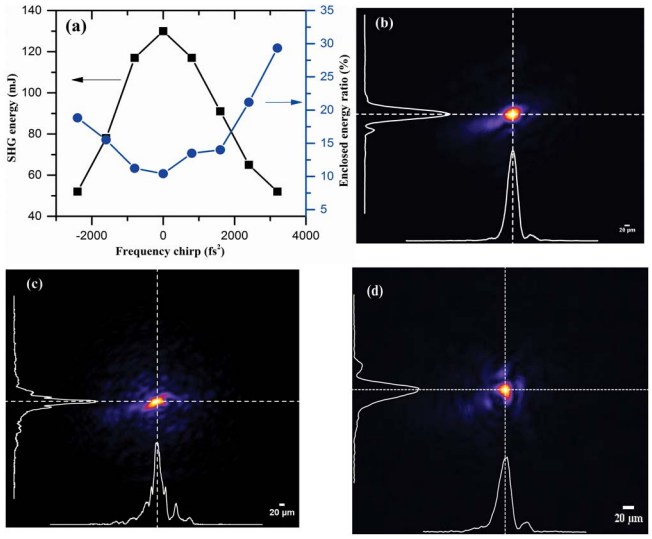

Fig. 2. Energy and focal spot quality of the scattering beam. (a) SHG energy and enclosed energy in $1/e^2$ diameter with different frequency chirps. (b) Focal spot of the FTL fundamental beam (800 nm). (c) Focal spot of the SHG beam converted from an FTL IR beam. (d) Focal spot of the SHG beam converted from an IR beam with $+3000 - \text{fs}^2$ chirp.

chirped-pulse amplification [9]. The experimental setup to generate high-energy γ-rays is shown in Fig. 1. The amplified 5 J beam from the laser system was divided into two using an 80% reflecting (20% transmitting) optical beam splitter. The reflected and transmitted beams are then transported into two pulse compressors. The reflected pulse with 80% of the total energy is compressed to 35 fs and is used to drive the LWFA electron beams. The transmitted beam, with 20% of the total energy, is also compressed and then upconverted to 400 nm by SHG in a nonlinear crystal (KDP, type-I phase matching).

The total fundamental pulse energy in the transmitted (scattering) beam was approximately 450 mJ, with a Fourier transform-limited (FTL) pulse duration of 35 fs. The conversion efficiency from 800 to 400 nm was measured at high power in vacuum for different chirps of the fundamental beam incident on the crystal. As shown in Fig. 2(a), conversion efficiency decreased for both positive and negative chirps on the incident pulse. It was highest for zero chirp, which is expected given the intensity dependence of the process. However, the focusability of the 400 nm light is crucial in the process of γ-ray generation by ICS as the latter depends on optimal spatial overlap between the electron beam and the focused scattering pulse, as well as the energy contained in the focus. Therefore, a trade-off exists between the conversion efficiency and the focusability of the 400 nm beam. Focusability is also susceptible to degradation from the nonlinear effects arising from the transmission of the 800 nm light through the KDP crystal.

Under our experimental conditions, the maximum B-integral was calculated to be 0.7 when the 70 mm-diameter fundamental beam, with 450 mJ at 35 fs, was transmitted through the 0.8-mm-thick KDP crystal. Measurements indicated that the B-integral did not affect the focal spot of the 800 nm beam, as shown in Fig. 2(b). However, severe distortion of the focal spot of the 400 nm beam was observed for zero chirp condition. The result, shown in Fig. 2(c), has enclosed energy in the $1/e^2$ diameter less than 10% of the incident energy and most of it is distributed outside the central focal spot. From this observation, it can be concluded that degradation of the focal spot arises primarily from the second-order nonlinear harmonic conversion process. However, other effects also contribute to this degradation, including the third-order nonlinear processes in the crystal, such as self-phase modulation (SPM). This arises from the fact that amplitude distortion is squared and the spatial phase aberrations are doubled for 400 nm as compared with 800 nm.

We performed a set of measurements to determine the focusability of the 400 nm beam as a function of chirp, to determine the optimal operating conditions for the ICS experiment. These studies indicated that, with a chirp of ± 3000 fs^2, the focal spot is 15 μm (FWHM), containing 30% of the energy in the $1/e^2$ diameter, as shown in Fig. 2(d). This spot size is close to optimal, based on prior studies conducted with 800 nm light. At this operating point, obtained by changing the grating-pair separation in the compressor, the pulse duration is 300 fs; 54 mJ of 400 nm light is produced by the SHG process. The use of lower power stretched pulses also reduces the risk of optical damage arising from SPM-induced inhomogeneity in the scattering beam line, and enables the use of high energy in the 400 nm beam to obtain the highest flux of γ-ray photons.The electron beams were generated via ionization injection [10,11] and subsequent LWFA in the gas-jet target. After compression to 35 fs duration [12], the drive laser pulses, with 2 J energy, were focused by a 1 m off-axis parabola to a 20-μm (FWHM) focal spot, with 40% energy enclosed in the FWHM contour. The focus was located on the rising edge of a 4-mm-long supersonic gas target (99% helium and 1% nitrogen) at a height of 1 mm above the nozzle. The electron plasma density, measured with a Mach–Zehnder interferometer, was 5×10^{18} cm^{-3}. The electron beam spectra were then

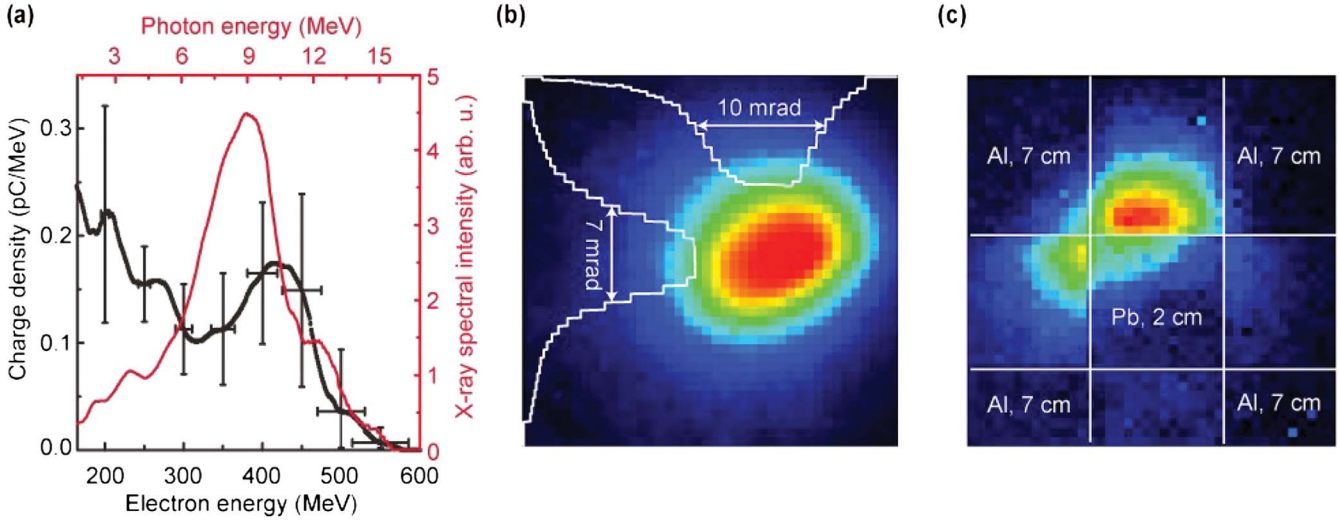

Fig. 3. Electron and γ-ray characteristics. (a) Black curve—averaged electron beam spectrum. The y error bars show standard deviations of charge density, whereas the x error bars show energy uncertainty due to pointing fluctuations. Red curve—corresponding estimated on-axis γ-ray spectral intensity (scattering laser pulse wavelength is 400 nm). (b) Measured signal on the CsI (background-corrected) with no spatial filter; γ-ray beam divergences (FWHM) are shown on the overlaid horizontal and vertical profiles. (c) Measured signal on the CsI (background-corrected). The overlay shows a spatial filter in front of the CsI, consisting of four blocks of aluminum (7 cm thick) and one block of lead (2 cm thick).

measured with a magnetic spectrometer, consisting of a 5.5-in. dipole magnet (0.7 T), and a fluorescent screen (LANEX), imaged by a 12-bit CCD camera. Due to space constraints, only electrons above 190 MeV could be detected. The electron beams had a charge of 53 ± 10 pC, an angular divergence of 4 ± 1 mrad, and an energy spectrum that extended to 550 MeV. A deconvolution process was applied to account for the divergence of the electron beam in calculations of the energy spectrum. Figure 3(a) (black line) shows the spectrum of the measured electron beams averaged (over 10 shots). The on-axis γ-ray spectral intensity, I_T, generated in the counterpropagating ICS geometry depends on the spectrum of the electron beam $f(\gamma)$ and is given by [13]

$$\frac{d^2 I_T}{d\omega d\Omega} \cong \frac{r_e mc}{16} N_0 a_0^2 \left(\frac{\omega}{\omega_0}\right)^{\frac{3}{2}} f\left(\gamma = \sqrt{\frac{\omega}{4\omega_0}}\right), \qquad (1)$$

where ω and ω_0 are scattered light (γ-rays) and laser frequencies, respectively, Ω is solid angle, r_e and m are the classical radius and mass of an electron, respectively, c is the speed of light, N_0 is the number of periods of laser pulse with which the electrons interact, and a_0 is the laser strength parameter (assumed to be $\ll 1$). Figure 3(a) (red curve) shows the calculated on-axis γ-ray spectrum, obtained using the measured electron spectrum. This spectrum peaks at 9 MeV and extends up to 15 MeV.

To detect γ-ray beams, we used a CsI(Tl) scintillator, imaged with a 14-bit EMCCD camera. The angular profile of the beam on the scintillator is shown in Fig. 3(b). Also shown are lineouts in the vertical and horizontal directions through the beam center that shows that the angular divergence of the beam is <10 mrad. To measure the γ-ray energy by means of attenuation, we placed a transmission filter in front of the CsI. The filter consisted of four aluminum blocks (7 cm thick) and one lead block (2 cm thick) arranged in a diagonal cross pattern, as shown in Fig. 3(c). We used the uncovered parts of the CsI to reconstruct un-attenuated γ-ray beam spatial profiles. This allowed us to make single-shot measurements of filter transmittances. We optimized the thicknesses of the blocks to achieve maximal change in transmittance differences in the 2–10 MeV range.

For the γ-ray beam shown in Fig. 3(c), we measured a transmittance of 0.61 ± 0.02 for the aluminum filters and 0.33 ± 0.05 for the lead ones. The simulated transmittances, based on the estimated γ-ray spectrum, were 0.62 and 0.34, respectively, which was in good agreement with the measurement. The difference between the transmittances measured (0.28 ± 0.05) corresponds to a γ-ray beam energy of 8^{+3}_{-2} MeV, close to the peak energy of the estimated γ-ray spectrum (9 MeV). Since the transmittance difference curve is almost linear in the 2–10 MeV range, and the expected shape of the γ-ray spectrum is symmetrical, this measurement estimates the averaged energy of the γ-rays produced. Based on the γ-ray spectrum and the known CsI detector response, it is inferred that 3×10^5 γ-ray photons per shot were produced. The measured x-ray photon number is found to be approximately consistent with the prediction of Eq. (1) using the measured parameters of the scattering laser beam and the electron beam, and assuming nonideal spatial overlap of the two beams (equal to ~1/3 of their beam diameters), which may arise from their pointing fluctuations.

In conclusion, we have demonstrated a >9 MeV γ-ray source by using the second harmonic of a high-power Ti:sapphire laser. A unique double-compressor and double-parabola interaction geometry enabled independent control of the LWFA process and allowed the optimization of the scattering beam parameters, while preserving the optimal spatiotemporal characteristics of the laser pulses.

This method can also be extended to scattering with higher laser intensities, allowing access to the nonlinear regime of ICS and the high harmonics of the γ-ray beam [14].

We thank K. Brown, J. Mills, and C. Petersen for their contributions to the laser facility. This material is based on work supported by the U.S. Department of Energy (DE-FG02-05ER15663), the Defense Threat Reduction Agency (HDTRA1-11-C-0001), the Air Force Office for Scientific Research (FA9550-11-1-0157), the Department of Homeland Security Domestic Nuclear Detection Office (HSHQDC-13-C-B0036), and National Strategic Research Institute (FA4600-12-D-9000). This support does not constitute an express or implied endorsement on the part of the government.

References

1. A. Compton, Phys. Rev. **21**, 483 (1923).
2. I. Pogorelsky, I. Ben-Zvi, T. Hirose, S. Kashiwagi, V. Yakimenko, K. Kusche, P. Siddons, J. Skaritka, T. Kumita, A. Tsunemi, T. Omori, J. Urakawa, M. Washio, K. Yokoya, T. Okugi, Y. Liu, P. He, and D. Cline, Phys. Rev. ST Accel. Beams **3**, 090702 (2000).
3. S. Y. Kalmykov, A. Beck, X. Davoine, E. Lefebvre, and B. A. Shadwick, New J. Phys. **14**, 033025 (2012).
4. E. Esarey, C. Schroeder, and W. Leemans, Rev. Mod. Phys. **81**, 1229 (2009).
5. H. Schwoerer, B. Liesfeld, H. P. Schlenvoigt, K. U. Amthor, and R. Sauerbrey, Phys. Rev. Lett. **96**, 014802 (2006).
6. K. T. Phuoc, S. Corde, C. Thaury, V. Malka, A. Tafzi, J. P. Goddet, R. C. Shah, S. Sebban, and A. Rousse, Nat. Photonics **6**, 308 (2012).
7. S. Chen, N. D. Powers, I. Ghebregziabher, C. M. Maharjan, C. Liu, G. Golovin, S. Banerjee, J. Zhang, N. Cunningham, A. Moorti, S. Clarke, S. Pozzi, and D. P. Umstadter, Phys. Rev. Lett. **110**, 155003 (2013).
8. N. D. Powers, I. Ghebregziabher, G. Golovin, C. Liu, S. Chen, S. Banerjee, J. Zhang, and D. P. Umstadter, Nat. Photonics **8**, 28 (2013).
9. C. Liu, S. Banerjee, J. Zhang, S. Chen, K. Brown, J. Mills, N. Powers, B. Zhao, G. Golovin, I. Ghebregziabher, and D. Umstadter, Proc. SPIE **8599**, 859919 (2013).
10. C. McGuffey, A. G. R. Thomas, W. Schumaker, T. Matsuoka, V. Chvykov, F. J. Dollar, G. Kalintchenko, V. Yanovsky, A. Maksimchuk, K. Krushelnick, V. Y. Bychenkov, I. V. Glazyrin, and A. V. Karpeev, Phys. Rev. Lett. **104**, 025004 (2010).
11. A. Pak, K. A. Marsh, S. F. Martins, W. Lu, W. B. Mori, and C. Joshi, Phys. Rev. Lett. **104**, 025003 (2010).
12. C. Liu, J. Zhang, S. Chen, G. Golovin, S. Banerjee, B. Zhao, N. Powers, I. Ghebregziabher, and D. Umstadter, Opt. Lett. **39**, 80 (2014).
13. P. Catravas, E. Esarey, and W. P. Leemans, Meas. Sci. Technol. **12**, 1828 (2001).
14. S. Corde, K. T. Phuoc, G. Lambert, R. Fitour, V. Malka, A. Rousse, A. Beck, and E. Lefebvre, Rev. Mod. Phys. **85**, 1 (2013).